THE JOURNAL OF PHYSICAL CHEMISTRY B

Article

pubs.acs.org/JPCB

Distinctions in Early Stage Unwinding Mechanisms of Zwitterionic, Capped, and Neutral Forms of Different α-Helical Homopolymeric Peptides

Prithvi Raj Pandey* and Sudip Roy

Physical Chemistry Division, National Chemical Laboratory, Pune 411008, India

Supporting Information

ABSTRACT: Molecular dynamics simulations of α-helical polyalanine, polyleucine, polylysine, and poly(glutamic acid) with different forms of terminal groups in water at 300 K showed sharp distinctions in their unwinding mechanisms. Zwitterionic, capped, and neutral forms of polyalanine, polyleucine, and polylysine have been explored to elucidate their unwinding mechanism at very early stage, e.g., initial time window. Role of water in the unwinding mechanisms of the various helices has been envisaged. Also, it is evident from our calculations that the short- and long-range nonbonded interactions among the side chains is an important factor determining the unwinding mechanisms of the various homopolymeric α-helices. These findings can be helpful in constructing predictive models for understanding of the unwinding of α-helical proteins and peptides.

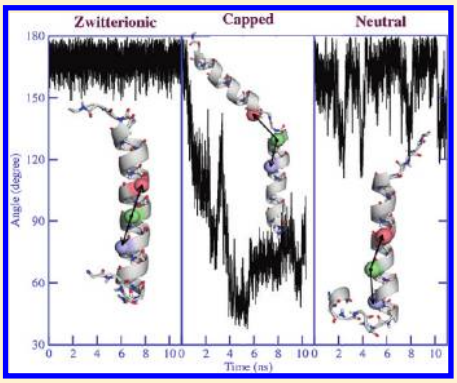

INTRODUCTION

Secondary structures of peptides and proteins refer to the highly regular local substructures. α-Helices are the most abundant secondary structure among all the secondary structures of protein. Hydrogen (H)-bonded structure of α-helix was first proposed by Pauling and Corey.[1] Since then, many studies have been performed to understand the stability of α-helices (ref 2 and references therein). H-bonding between the carbonyl oxygen (C═O) of *i*th residue and amide hydrogen (NH) of *i*+4th residue on the peptide backbone gives the peptide chain a α-helical structure. Being the most available secondary structure, understanding of the unwinding mechanism of α-helices may augment our understanding of protein unfolding.

Experimental and theoretical studies have been performed to understand the structure, stability, and dynamics of helices. Kemp et al. have performed a series of studies on helices using ^{1}H NMR, ^{13}C NMR, and also CD spectroscopic techniques.[3−5] Zagrovic et al. have measured the radii of gyration of alanine-based peptides using synchrotron radiation and the small-angle X-ray scattering techniques.[6] They have also analyzed the discrepancies using the analytical Zimm−Bragg−Nagai theory and with molecular dynamics (MD) simulations. Podtelezhnikov et al. have shown the influence of H-bonding on polyalanine conformations using Metropolis Monte Carlo procedure for protein modeling.[7] Agostini et al. have used generalized simulated annealing method coupled to the GROMOS96 molecular force field to find the minimum-energy conformation of polyalanine.[8] Recently, Diana et al. have studied the thermal unfolding of a 15-mer endothelial growth factor mimicking α-helical peptide through combination of computational and spectroscopic analysis.[9] Asciutto et al. have further studied the AP peptide (a 21-residue ALA-rich peptide) and have observed unwinding from the terminal of the helical chain.[10]

α-Helical peptides of only one type of amino acid, i.e., homopolymeric, have been studied in the past to understand various properties of a helical structure. Helical propensities of various amino acids have been defined by studying different homopolymeric peptides (ref 2 and references therein). Sorin et al. have chosen capped polyalanine and Fs peptide (α-helical arginine substituted analogue of capped polyalanine) in their study to understand helix−coil transitions.[11] Garcia et al. have studied the effect of implicit and explicit solvation on helix−coil transition and established force fields.[12−14] MD simulations have proved to be an useful tool in understanding the mechanism of helix formation, its stabilization, and disruption.[15]

In our previous report, we have studied the early-stage unwinding mechanisms of only zwitterionic α-helical polyalanine (PA), polyleucine (PL), and polylysine (PLY) in water at 300 K using classical MD simulations.[16] We have proposed that the unwinding of 30 amino acid long chain of zwitterionic α-helical PA, PL, and PLY is triggered by higher fluctuations of the terminal residues. The unwinding is relayed from the terminals to the middle for PA and PL, but not for PLY. After the initial unwinding from the terminals, the PLY helix broke in the middle due to interresidual H-bonding in the side chain. In continuation of the study of zwitterionic forms of PA, PL, and

Received: November 27, 2011
Published: March 26, 2012

PLY, here we report the similarities and dissimilarities of early-stage unwinding mechanisms of the capped and neutral forms of these helices. We have also studied the unwinding mechanisms of zwitterionic, capped, and neutral poly(glutamic acid) (PG) helices in the present report. The C- and N-terminals were capped with $-NHCH_3$ and $-COCH_3$, respectively, in all the capped helices. The terminals were kept as $-NH_2$ and $-COOH$ in all the neutral helices. These are compared with the zwitterionic helices where the terminal residues were taken as $-COO^-$ and $-NH_3^+$. The primary motivation to study the unwinding mechanism of the different forms of the homopolymeric α-helical peptides is to gain information for designing stable helical peptides in the future to understand the diseases caused due to unwinding of protein, protein−drug interactions, and other biological phenomena. Know-how of such unwinding can help in developing predictive models for determining early-stage unwinding positions of α-helical peptides and proteins. We are systematically targeting to elucidate the unfolding behavior of amino acids in their own environment as a step forward to understand the early-stage unwinding of naturally occurring proteins and peptides.

Here we have considered four different 30 amino acid long polypeptides PA, PL, PLY, and PG and their three different forms—zwitterionic, capped, and neutral. To check the statistics, we perfomed three independent simulations of these helices in water and have proposed their unwinding mechanisms. The results of one set of simulations are given here and rest are included in the Supporting Information (SI). ALA and LEU were considered because of their higher helix-forming propensity among amino acids with hydrophobic alkyl side chain.[17] Additionally, their polymers PA and PL differ in the degree of side-chain hydrophobicity as ALA has methyl and LEU has isobutyl group as side chain. PLY contains $-NH_2$ group in its side chain which is hydrophilic in nature. The purpose of choosing the polymer of glutamic acid in the present study is to compare the unwinding mechanisms of the PG helices with the PLY helices. LYS contains $-NH_2$ group in its side chain, and we have observed that interresidual H-bonding among these side-chain $-NH_2$ groups influence the unwinding mechanism of zwitterionic PLY helix. GLU contains propanoic acid ($-(CH_2)_2-COOH$) group in its side chain. Thus, there exists a possibility of formation of interresidual H-bonding among the side-chain $-COOH$ groups in the PG helices. Apart from this, the effect of the short-length hydrophobic spacer group ($-(CH_2)_2$) and hydrophilic side chain in PG can be explored on the early stage unwinding mechanism. LYS contains *n*-butylamine ($-(CH_2)_4-NH_2$) group in its side chain. However, the hydrophilic character is similar in the GLU and LYS side chains. The zwitterionic PLY and PG with side chain as $-NH_2$ and $-COOH$, respectively, are physically difficult to synthesize, so they are only of theoretical interest. This is because the PLY side chain and PG side chains can remain as $-NH_2$ and $-COOH$ only at a high and low pH, respectively. But at high pH the N-terminal cannot remain as $-NH_3^+$ and at low pH C-terminal cannot remain as $-COO^-$. Such a condition is difficult to achieve experimentally. However, such forms of PLY and PG serve our purpose of introducing hydrophilic groups with different spacer groups length in the side chain to understand its effect on the unwinding mechanism of helices containing different terminal groups.

Sharp distinctions have been observed in the unwinding mechanisms of polypeptides with the change in terminal groups. The neutral forms of the helices containing hydrophobic side chains, i.e., PA and PL tend to unwind from the terminals similar to their zwitterionic analogue and this unwinding is relayed to the middle. Their capped forms start to unwind from the terminals, which is not relayed further to the middle. PLY helices of all the forms (zwitterionic, capped, and neutral) with hydrophilic side chain unwind from the middle. All the forms of PG helices unwind from the terminals. The mechanism determining this interesting distinction in the early stage unwinding pathways has been investigated for the first time in this report.

The role of water in the unwinding of α-helical peptides has been studied in the past by DiCapua et al.[18,19] H-bond exchange method is an useful tool to understand the H-bonded structures in proteins.[20] Several approaches taken to realize the relation between solvation and peptide folding have been explained by Baldwin.[21] An α-helix unwinds in water due to the exchange in intrabackbone H-bonding between C═O of *i*th and NH of *i*+4th residue with H-bonding with water. In the present study, we have also investigated the role of water in the unwinding mechanism of the different helices.

COMPUTATIONAL METHODS

All the simulations were performed using GROMACS 4.0.7 package.[22,23] All-atom OPLS force field[24] has been used for the study. In our previous study,[16] we performed the calculations with Amber force field[25] also and showed that Amber overstabilizes the helix but produces the same result in a longer time scale for zwitterionic helices. All the peptide helices were first energy minimized using steepest descent method to relax the angles and dihedrals. Then, all the systems were constructed by placing the energy-minimized peptide in the middle of the simulation box, maintaining a distance of 2 nm from the walls of the box. Then, the peptide helix was solvated with water. Explicit TIP3P[26] water model has been used in the study as it is the most acceptable water model for studying biomolecules. Further, a 2 ns equilibration run was performed with the peptide being position restrained. This allowed the water molecules of the system to equilibrate and organize themselves around the peptide. Finally, the position restraint was taken off and trajectories were recorded for 30 ns for further analysis. Three independent sets of simulation for each case, i.e., zwitterionic, capped, and neutral, were performed with different initial configuration of water molecules. The initial velocities were also different for all these different simulation sets.

This report primarily deals with the understanding of early-stage unwinding mechanisms of various forms of homopolymeric α-helices. In this 30 ns time scale, various conformational changes were obseved for the helical peptides; unwinding and potential rewinding also take place in this time scale. Thus, the simulation time of 30 ns provides us ample scope for further analysis. Isothermal and isobaric ensemble (NPT) and periodic boundary conditions (PBC) were used. Temperature was kept constant at 300 K for all the three systems using v-rescale thermostat. Isotropic pressure coupling was applied using Berendsen barostat[27] for all three systems. Bonds were not constrained and a time step of 1 fs was used for the simulations. For Lennard-Jones interaction, a cutoff at 1.0 nm was applied; electrostatic interactions were taken care of with particle mesh Ewald (PME)[28] method with a real space cutoff of 1.0 nm. Trajectories were analyzed to calculate root-mean-square fluctuations, and radial distribution functions. All other analysis

dx.doi.org/10.1021/jp301556x | J. Phys. Chem. B 2012, 116, 4731−4740

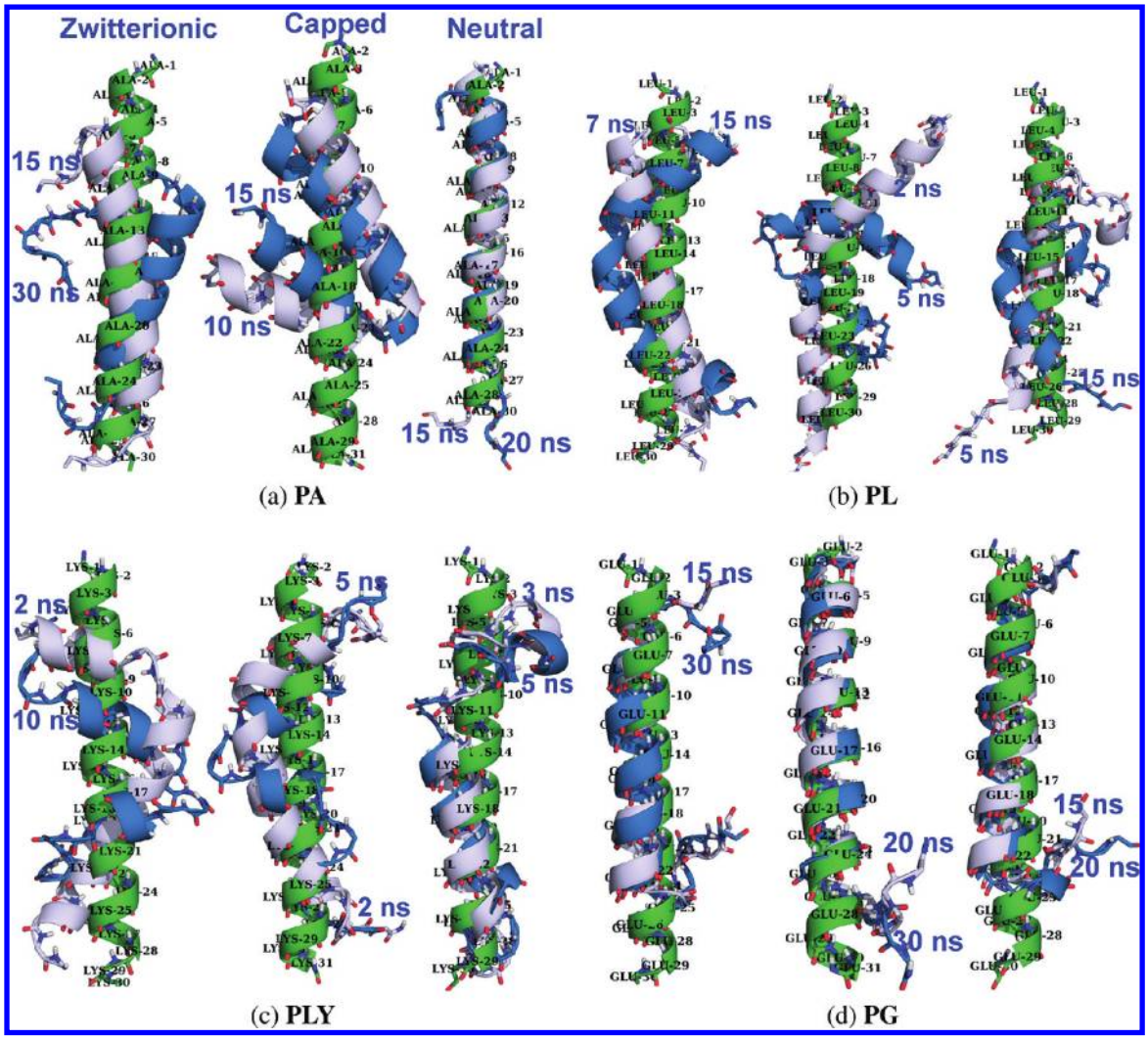

Figure 1. Snapshots at different times for (a) PA, (b) PL, (c) PLY, and (d) PG helices. Water and side chains have not been shown for simplicity. 0 ns is shown in green in all the systems. Other colors corresponding to other times are indicated in the figures. The order of zwitterionic, capped, and neutral from left to right is maintained in all the systems similar to the PA system.

methods have been described along with results and discussion. The potential energies as a function of time (30 ns) for all the forms, for the simulation set reported in the main text, have been checked and depicted in the Supporting Information to confirm that there is no phase change in this period of time (Figure S1).

RESULTS AND DISCUSSION

We report here the unwinding mechanisms of various forms of PA, PL, PLY, and PG helices. The unwinding mechanisms of zwitterionic forms of PA, PL, and PLY helices were included in our previous report;[16] here we report the unwinding mechanisms of the neutral and capped forms of PA, PL, and PLY. In addition to neutral and capped forms, the zwitterionic form of PG has also been reported in the present study and a systematic comparison has been performed.

Position and Time Scale for Unwinding of the Helices. Noticeable distinctions have been observed in the unwinding pathways of the various helices with the change in terminal groups. Snapshots at various times for the different systems have been shown in Figure 1. Water and side chains of the amino acids have not been shown for simplicity. The capped forms of both PA and PL appear to unwind from the middle of the α-helical chain (Figure 1, a and b). The neutral and zwitterionic forms of both of these α-helices unwind from terminals (Figure 1, a and b). All the forms of PLY unwind from the middle of the helical chain (Figure 1c). Snapshots of zwitterionic, capped, and neutral forms of PG are shown in Figure 1d. All the forms of PG appear to be unwinding from the terminals in the initial 30 ns (Figure 1d).

The time scales of the unwinding of different helices have been estimated from the distribution of distance between C═O of *i*th and NH of *i*+4th residues as a function of time shown in Figure 2. Since H-bonding between C═O of *i*th and NH of *i* +4th residues is responsible for the α-helical structure of a peptide, the distance distribution as a function of time gives the estimation of the time scale of the breaking of such H-bonds. The distance between C═O of residue 1 and NH of residue 5, and C═O of residue 11 and NH of residue 15, were first calculated and the distributions were plotted averaging over each 2 ns interval of time for the systems. All the distance distributions were averaged over number of frames in the 2 ns interval of time. The capped PA and PL helices unwind from the middle (see Figure 1a,b). Therefore, the distance distributions between residues 11 and 15 for these helices move away from H-bonding distance much earlier than the

dx.doi.org/10.1021/jp301556x | J. Phys. Chem. B 2012, 116, 4731−4740

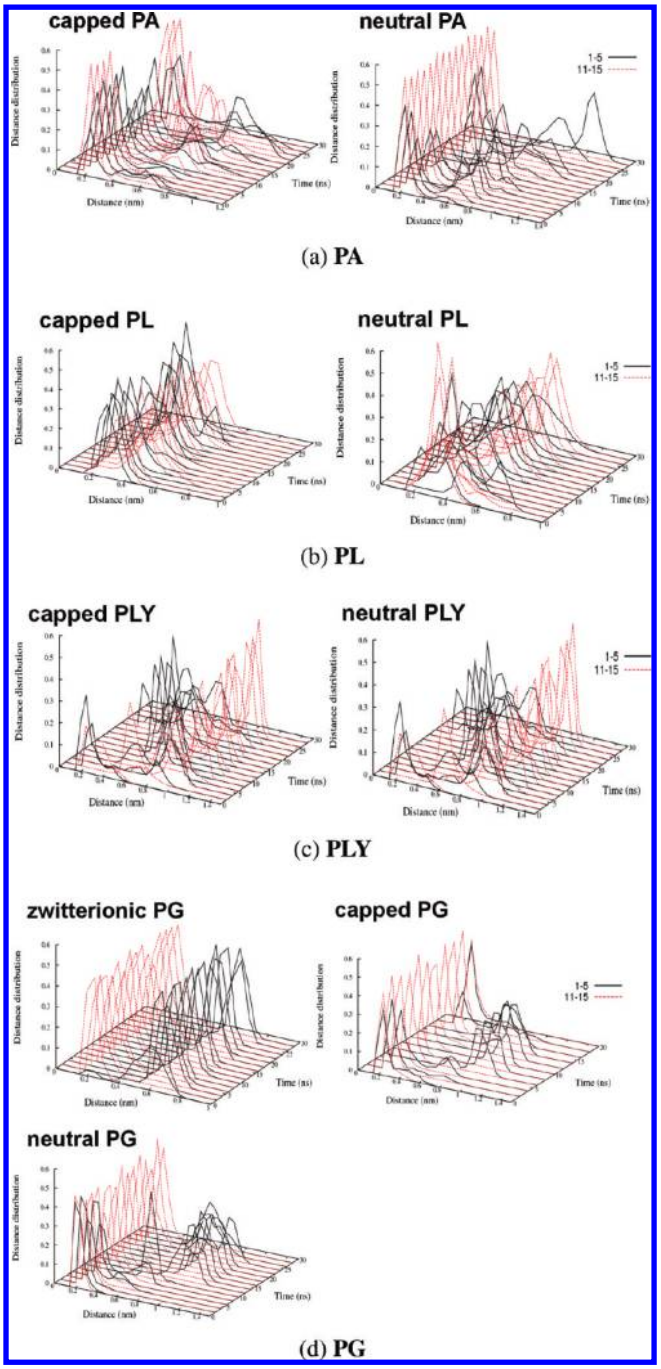

Figure 2. Distribution of distance between C═O of residue 1 and NH of residue 5 and between residues 11 and 15 plotted against time for (a) PA, (b) PL, (c) PLY, and (d) PG helices.

distance distributions between residues 1 and 5 (Figure 2a,b). This shows that the middle residues unwind much earlier than the terminal residues for capped PA and PL helices. But, for neutral PA and neutral PL helices (Figure 2a,b) the case is opposite. This shows that the neutral PA (in nearly 8 ns) and neutral PL (in nearly 2 ns) start to unwind from the terminals as in the case of zwitterionic PA and PL.[16] Further, similar distance distribution plots for all the forms of PLY (zwitterionic[16]) show that it unwinds from the middle of the α-helical chain (Figure 1c) on a time scale of initial 2−3 ns. Similar distance distributions were also plotted for the other two simulation sets and are depicted in the Supporting Information (Figures S3 and S4). In some of the cases, a difference of 2−4 ns has been observed in the unwinding time scales, but the mechanism of unwinding remains the same. All the forms of PG helices are observed, from the snapshots, to be unwinding from the terminals (Figure 1d) but none of them unwinds completely in the 30 ns simulation time. The distance distributions of PG between residues 1 and 5 are seen to be moving away from H-bonding distance at very early stage for all the forms of PG helices (Figure 2d). But the distance distributions between residue 11 and residue 15 do not shift from H-bonding distance in 30 ns (Figure 2d). A shift in the distance distribution plot for neutral PG in the second simulation set can be observed around 24 ns time scale (Figure S3). In the present context where we are interested in understanding the early-stage unwinding mechanism of the helices, the pattern of unwinding of PG is clear in this time scale of 30 ns.

Fluctuations and Unwinding. Unwinding of the helices from terminals can be attributed to the higher fluctuation of the terminal residues. To check this, we have investigated the relationship between unwinding of the various helices to the fluctuations of the residues present in the respective helices. Root mean square fluctuation (RMSF) of the (C_α) carbons of helical backbone has been plotted in Figure 3. All these RMSF plots have been calculated for certain intervals of time, i.e., 0−1, 1−2 ns etc. The intervals were chosen depending upon time scale of unwinding of the investigated helices as observed from the distance distribution from Figure 2.

For both capped and neutral PA helices the intervals were chosen to be 5 ns (Figure 3a). The capped PA helix unwinds completely in 30 ns, but not the neutral PA helix. It is evident from the snapshots that the capped PA helix unwinds from the middle of the α-helical chain (Figure 1a). RMSF for the (C_α) carbons of terminal residues is the highest in the first interval, i.e., 0−5 ns for capped PA (Figure 3a). Further as the time increases, the RMSF of (C_α) carbons of the middle residues increase and become almost equal to the RMSF of N-terminal residue. Asymmetry in the unwinding is visible in the 0−5 and 5−10 ns intervals as the RMSF of the residues near C-terminal (residue 30) is higher than that of N-terminals (residue 1). However, for neutral PA helix the RMSFs of the terminal residues are higher in all intervals (Figure 3a). The asymmetry in RMSF is visible in some cases in some particular time intervals, e.g., 25−30 ns for neutral PA. Though the unwinding of neutral PA is not complete in the 30 ns time scale, the early-stage pattern of unwinding is distinct from the terminals of the α-helical chain. Zwitterionic PA shows the similar property as reported earlier.[16] Similar to PA, capped and neutral helix of PL unwind from middle and terminals, respectively (Figure 1b). But the time scales of unwinding of PL helices are different from those of PA helices (Figure 2). Capped PL unwinds completely within 10 ns and the neutral PL in 30 ns. Thus, the intervals selected for plotting RMSFs were 1−10 ns for capped PL and 5−30 ns for neutral PL (Figure 3b). The RMSFs of the middle residues are almost similar to those of the terminal residues in the 0−1 ns interval for capped PL (Figure 3b). The RMSFs of the middle residues further increase in the 2−3 ns interval. This validates the unwinding of the capped PL helix from the middle of the α-helical chain triggered by the fluctuation in the middle residues. For neutral PL helix the RMSFs for the terminal residues are distinctly higher than the middle residues in the 0−5 ns interval (Figure 3b) and the helix breaks from the terminal. A sharp drop in the RMSFs of the N-

dx.doi.org/10.1021/jp301556x | J. Phys. Chem. B 2012, 116, 4731−4740

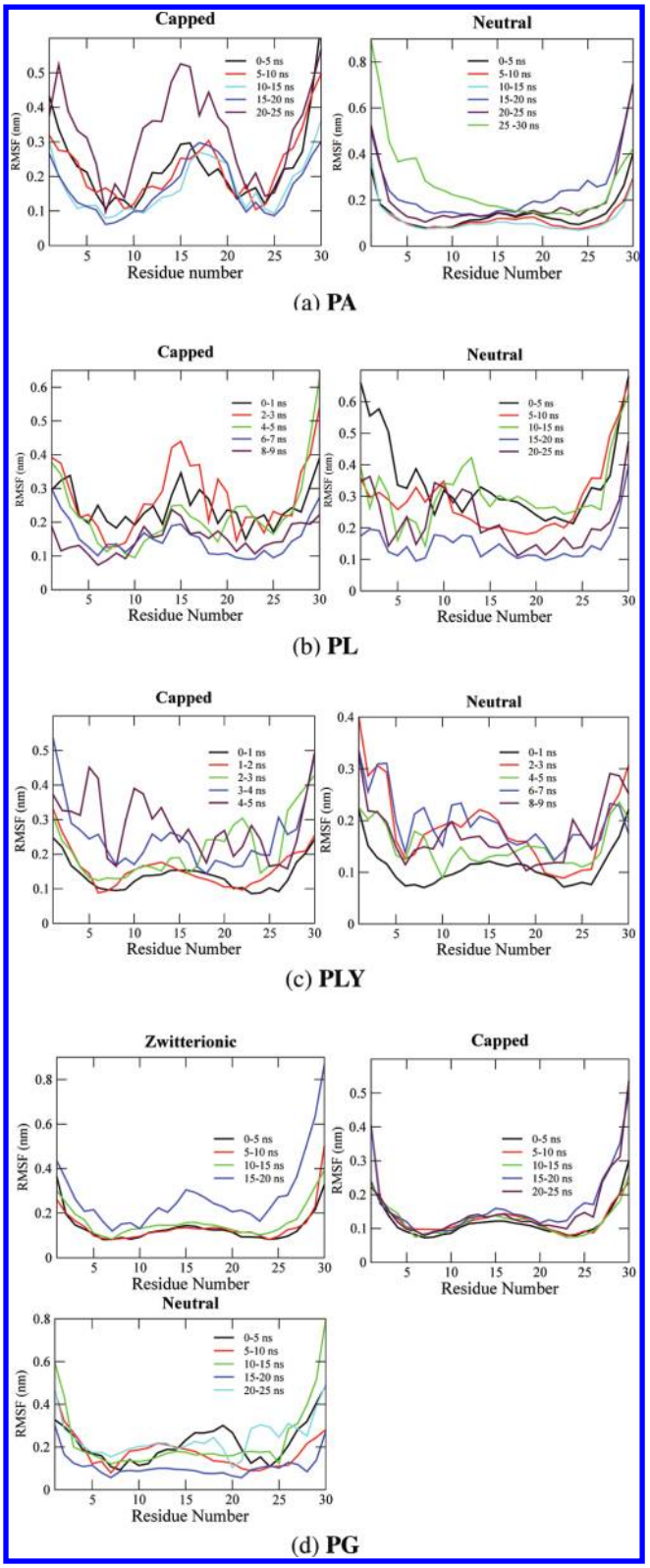

Figure 3. RMSFs of C_α carbons on the helical backbone at different intervals of time for (a) PA, (b) PL, (c) PLY, and (d) PG helices.

terminal residues can be observed in the 5−10 ns compared to 0−5 ns interval. This is possibly because of the rewinding in that time interval for these residues.

The zwitterionic α-helical PLY starts to unwind from the terminals because of higher fluctuations of the terminal residues, but the unwinding is not relayed to the middle of the α-helical chain.[16] Instead, the side-chain $-NH_2$ groups of lysine form interresidual H-bonds and the helix breaks in the middle. We have also observed for both neutral and capped PLY helices; the RMSFs (Figure 3c) of the terminal residues are higher than the middle residues in the first intervals. With increasing time the fluctuations of the middle residues keep increasing. However, the snapshots for both neutral and capped PLY helices (Figure 1c) suggest unwinding from middle of the α-helical chains. Similar RMSFs have been calculated and depicted in Figure 3d for zwitterionic, capped, and neutral PG helices. All forms of PG helices do not completely unwind in the 30 ns time scale. But, unwinding and rewinding to the α-helical state has also been observed in the 30 ns time scale for all the forms of PG helices. The RMSFs for the terminal residues are higher than for the middle residues in all intervals of time for all the forms of PG (Figure 3d). Therefore, the unwinding pattern remain same even after rewinding for all forms of PG helices; i.e., all the helices unwind from the terminals (Figure 1d). Higher fluctuations of the terminal residues trigger the unwinding process for all forms of PG helices. Asymmetry in RMSF for terminal residues can again be observed here because the RMSFs of the C-terminal (residue 30) residues attain higher values than the RMSFs of N-terminal (residue 1) residues in the same intervals of time (Figure 3d) for all the forms of PG helices. This is also visible in the snapshots of the PG helices (Figure 1d).

Radial distribution function (RDF) plots are depicted in Figure 4 to understand the side-chain and main-chain H-bonding in PG and PLY helices. For all the forms of the PLY and PG helices the main chain RDFs were plotted between C═O and NH of the peptide backbone. Side-chain RDFs were plotted between N and H of the side-chain $-NH_2$ groups for PLY and between oxygens and H of the side-chain −COOH groups for PG. All the RDFs are averaged over certain intervals of time, i.e., 1 ns for PLY and 5 ns for PG. From Figure 4a the side-chain RDF peaks (first peak) for all the forms of PLY are clearly visible to be increasing with time and in the same time scale the main-chain RDF peaks are decreasing. This suggests that the unwinding of all the forms of PLY helices from the middle of the α-helical chain is driven by interresidual H-bonding among the side-chain $-NH_2$ groups. On the contrary, there is almost no indication of interresidual H-bonding among the side-chain −COOH groups in any form of the PG helices (Figure 4b). There is almost no change in the first RDF peaks with increase in time. There is, however, a small drop in the peak heights for the main-chain RDFs of PG helices because of the unwinding of the helices, though they are from the terminals. The inability of the PG helices to form interresidual side-chain H-bonds can be attributed to the lower length of the side chains in PG than in PLY. Possibly because of long flexible side chains, PLY helices attain the proper orientation to create side-chain H-bonding.

Role of Water on Unwinding of Helices. The secondary structure of high-propensity α-helical peptides stays as α-helix primarily because of the H-bonding between carbonyl oxygen (C═O) of the ith and amide hydrogen (NH) of the i+4th residue of the backbone. These H-bonds can be exchanged with the surrounding solvent (in this case water) to unwind the α-helical peptides. DiCapua et al. have shown that for such an exchange of hydrogen bonding, water molecules must enter the accessible regions inside the helical backbone.[18,19] Li et al. have studied the effect of solvation and side-chain modulation on the

dx.doi.org/10.1021/jp301556x | J. Phys. Chem. B 2012, 116, 4731−4740

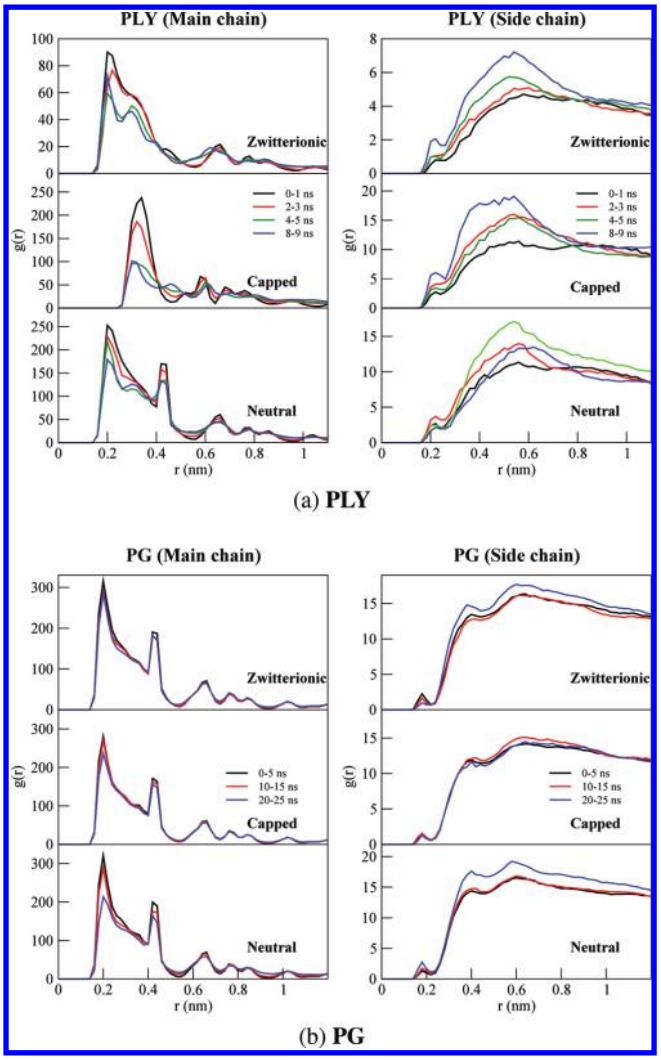

Figure 4. RDF among the (a) side-chain NH_2 groups for PLY helices and (b) side-chain −COOH groups for PG helices at different intervals of time.

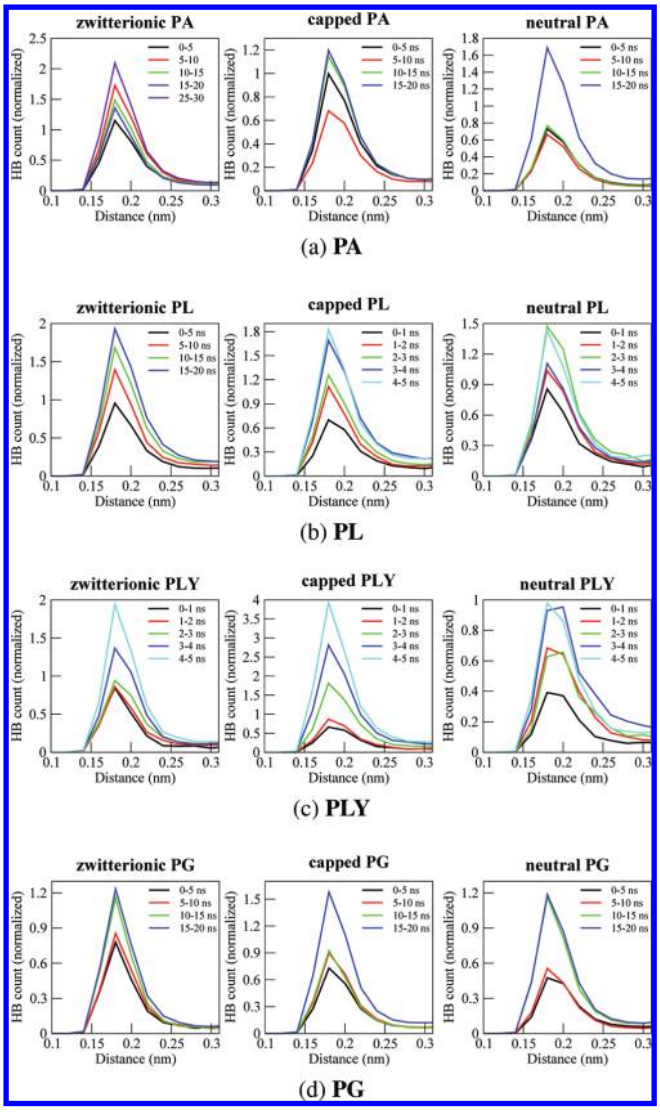

Figure 5. Count of the number of H-bonds among backbone NH and water oxygen at different intervals of time for (a) PA, (b) PL, (c) PLY, and (d) PG helices.

peptide backbone conformation using a model peptide $AcGGAGGNH_2$.[29] Therefore, the role of water in the unwinding of the different helices becomes important. In the present study, the initial 2 ns position restrained simulations for all the systems allow the water molecules to equilibrate and settle around the α-helix. So water molecules are present in the accessible regions around the α-helical backbone in the initial conformation from which we have started to record the trajectory for analysis.

To understand the effect of water on the unwinding of the α-helical chain, the count of water molecules forming H-bond with the backbone NH has been plotted as a function of the distance between water oxygen (OW) and NH in Figure 5 for all the systems. The distribution of the H-bond count as a function of distance has been calculated in the following manner. Initially, the distances between all the NH and OW in a polypeptide were calculated in all the frames for each interval of time. Then the donor−hydrogen−acceptor (N−H−OW) angles were computed for all the water molecules confined between 0.1 and 0.4 nm from NH. Among them, only those water molecules were counted for which the N−H−OW angle was greater than 150° considering the linear nature of the H-bond. Subsequently, the normalized count of hydrogen bond distances has been depicted as a histogram with respect to the NH−OW distance. All these distributions were plotted for certain intervals of time similar to the other plots reported. It is observed from Figure 5 that the height of the peaks of the distributions are increasing with the increment in time for all the systems. This confirms that formation of H-bonds between the peptide backbone and water increases with time. Only for capped PA, the peak height of the distribution decreases at 5−10 ns interval (Figure 5a) may be because some rewinding to the helical form happens in this interval. However, after this interval the peak height increases like other forms of helices. H-bond count distribution peak increases continuously in all the intervals for capped PL (Figure 5b). However, for neutral PL a drop in the peak height can be observed in the 3−4 ns interval (Figure 5b). Peak heights of capped PLY also increase with time (Figure 5c). Notably, the peak height in the last (4−5 ns) interval for capped PLY is the highest among all the systems studied. This is because capped PLY unwinds completely in 5 ns and higher amount of unwinding implies higher probability of H-bonding between NH and OW. For neutral PLY also the peak heights increase, but the peak heights are similar in the 1−

dx.doi.org/10.1021/jp301556x | J. Phys. Chem. B 2012, 116, 4731−4740

2 and 2−3 ns intervals and also in 3−4 and 4−5 ns intervals. This implies that in these intervals the amount of helix unwinding and hence the probability of H-bond formation between NH and OW are similar. All the PG systems have the highest unwinding time scale among the homopolymeric helices studied here. Any of the PG helices do not completely unwind in the 30 ns time scale (Figure 1d). Zwitterionic PG unwinds with steady increase in the H-bond count in all the intervals (Figure 5d). Capped PG shows a sharp increase in the peak height in the 15−20 ns interval, and the neutral PG shows a sharp increment in the 10−15 ns interval (Figure 5d). The unwinding of the helical chain has some correlation with the H-bond count because in the same time scale helices also start to unwind. In Figure 6 we have elucidated the correlation between

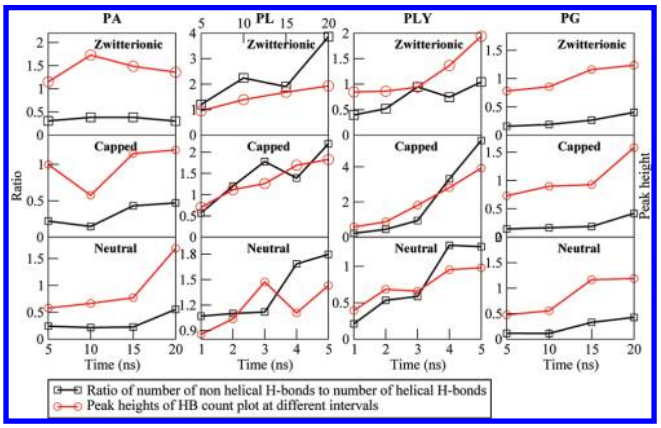

Figure 6. Ratio of number of nonhelical H-bonds (C═O of *i*th and NH of *i*+4th residue) to number of helix-forming H-bonds for all the systems plotted against time. Also the peak heights at different intervals of time in Figure 5 have been plotted as a function of time. The plot of zwitterionic PL is depicted in the 20 ns time scale, but capped and neutral PL are depicted in the 5 ns time scale.

the hydrogen bond count and change in helicity as a function of the same intervals of times. Change in helicity is calculated as a ratio between the number of nonhelical H-bonded (within the backbone) residues and H-bonded residues. We have set a similar criterion to count the H-bonded residues as above. In this plot (Figure 6), the count of the H-bond is nothing but the maxima of H-bond count distribution of Figure 5 for all the systems. The correlation between the probability of H-bond formation between the solvent water and the change in helicity is evident from all the systems as we observed from Figure 5. Whenever there is a higher ratio of unwinding versus rewinding, the distribution of H-bond distance increases like in neutral PA shows a sharp jump in the peak height in 15−20 ns interval (Figure 5a). The jump is due to the maximum amount of unwinding in that time scale (Figure 6). Capped PA shows a dip in the peak height in the 5−10 ns interval due to rewinding as we have predicted from the H-bond distribution. In the case of neutral PA there is an increase in helicity (rewinding) observed in the interval of 3−4 ns, but the H-bond count increases. This may be because of the faster dynamics of the system. For all the forms of PG, PA, and PLY, the correlation is highly satisfactory. Similar correlations have also been investigated for the other two simulation sets (Figure S5 in the Supporting Information). Though there is a small difference in the unwinding time scales, the H-bond formation probability among backbone and water molecules and the change in helicity are highly correlated in the other two simulation sets also.

The measure of average H-bond count is a useful quantity to understand the relation between unwinding of helix and the effect of water on it. But the driving force for exchange of H-bonding within the α-helical backbone with water cannot be understood by this. H-bonding is primarily an electrostatic interaction. Thus, to understand the exchange of H-bonding within the α-helical backbone with water, electrostatic interaction energy for the H-bonding between C═O of the *i*th and NH of the *i*+4th residue has been calculated and compared with the H-bonding energy between NH and OW (represented by dotted line) in Figure 7. For computing these

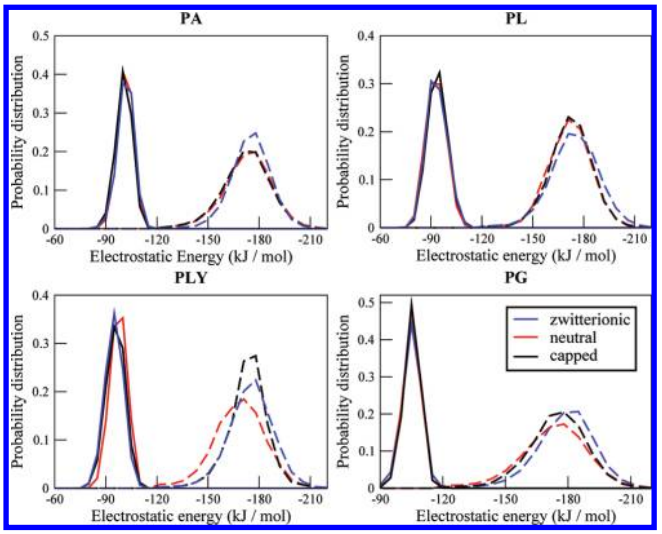

Figure 7. Distribution of electrostatic interaction energy of interaction between backbone C═O and NH (solid line), and between NH and water (dashed line).

energies, the Coulombic interaction potential energy among the concerned atoms has been used, i.e., $q_i q_j/4\pi\varepsilon_0 r_{ij}$, where q_i and q_j are the charges on the concerned atoms and r_{ij} is the distance between them, and ε_0 is the permittivity of free space. In our simulations the term ε_r (permittivity of the medium) is always 1 as the long-range electrostatic interactions were taken care by using PME. The term $1/4\pi\varepsilon_0$ is equal to 138.935 485 kJ mol^{-1} nm e^{-2}. To calculate the electrostatic interaction energy for the H-bonding between C═O of the *i*th and NH of the *i* +4th residue, first the r_{ij} among all these pairs were computed and then the energy was calculated only for pairs which have N−H···O angle more than 150° and r_{ij} was between 0.1 and 0.4 nm. Further, the total energy was normalized by the number of residues and frames. Finally, the normalized distribution of the energy was plotted averaging over the time scale of early-stage helix unwinding, e.g., 15 ns for capped PA and 5 ns for capped PL. The higher range of r_{ij} as H-bond criteria was chosen to be large as we have observed in Figure 2 that the H-bonding distances of the backbone keep fluctuating within this range. Further, for calculating the electrostatic interaction energy for the H-bonding between NH and OW, the same H-bond distance range has been used as in Figure 5.

The interaction energy between NH and OW (represented by the dashed line) is lower than the energy between C═O of the *i*th and NH of the *i*+4th residue (solid line) in the helical backbone for all the systems (Figure 7). From this, we can infer that the unwinding of the helices is favored by the more

dx.doi.org/10.1021/jp301556x | J. Phys. Chem. B 2012, 116, 4731−4740

stabilizing H-bonding interactions between NH and OW than the intrahelical H-bonding interactions. There is not much difference in the distribution peaks of electrostatic energies for the intrahelical H-bonding interactions of capped and neutral systems. This may be because the charges on C═O ($q_{C=O}$ = −0.5) and NH (q_{NH} = 0.3) for all the helices studied here are the same in the OPLS-AA force field. The end groups were not taken into account in any of these distributions. Charge on OW for TIP3P water model is −0.834. Thus, there is not much distinction between the distributions of interaction energies among NH and OW for all the helices except PLY. Peak of the capped PLY appears at considerably higher value than neutral PLY. This is due to the fact that the capped PLY has the highest distribution of H-bond count (Figure 5c). Thus, the higher probability of H-bonding due to the favorable H-bond electrostatic energy translates to the highest unwinding. The peak distribution for electrostatic energy between NH and OW is broader than similar energy between C═O of the *i*th and NH of the *i*+4th residue. This indicates the fluctuations in the energy values are larger for H-bonding interactions between NH and OW than the intrahelical H-bonding interaction. To show this, energies as function of time has been included and discussed in the Supporting Information (Figure S2). The energetics of peptide H-bonds have always been thought of as a very important criterion in helix formation right from the time when the H-bonded structure of α-helix was proposed by Pauling and Corey.[1] After that, various approaches have been adopted to understand the relation between solvation and peptide folding.[21] Doruker et al. have shown that the effect of water on helices is highly residue specific.[30] Electrostatic solvation free energy calculations have been performed in the past to understand the role of interaction between helical peptide groups and water in determining helix propensities.[31,32] Here, we have taken the simple approach of calculating the electrostatic potential energies for intrahelical H-bonding interactions and interaction of helical backbone with water to understand the driving force for helix unwinding in water.

Distinction of the Helix Unwinding Sites. Calculation of the electrostatic energies shows the possible driving factor for unwinding of the different helices but it does not clarify the unwinding of the different helices at different sites, i.e., middle and terminals. RMSFs (Figure 3) for each variants have shown that fluctuation play a role to trigger the unwinding process. Still the question remains what is the extent of this fluctuation to dictate the process of unwinding sites. Therefore, we have calculated the angle between two vectors, between the C_α carbon of residue 15 and the C_α carbon of residue 11 and the vector between the C_α carbon of residue 15 and the C_α carbon of residue 19; i.e., the vectors constitute the helical turn at the middle of the α-helical chain and are plotted as function of time in Figure 8. All the systems in the plot show the starting angle of nearly 180° between the vectors, which is obvious as the starting structures are prefect α-helical. As the time increases the angle starts to fluctuate and in some cases moves quite far from linearity (i.e., 180°). We have already observed in the snapshots that the capped PA and PL helices seem to unwind from the middle of the α-helical chain and the neutral form from the terminals (Figure 1a,b). The zwitterionic forms of these two helices were also observed to unwind from the terminals.[16] In Figure 8 we see that for PA the angle fluctuations between the vectors are less for zwitterionic and neutral forms than for the capped PA in the early stages. Further, similar results for the three forms of the PL helices can

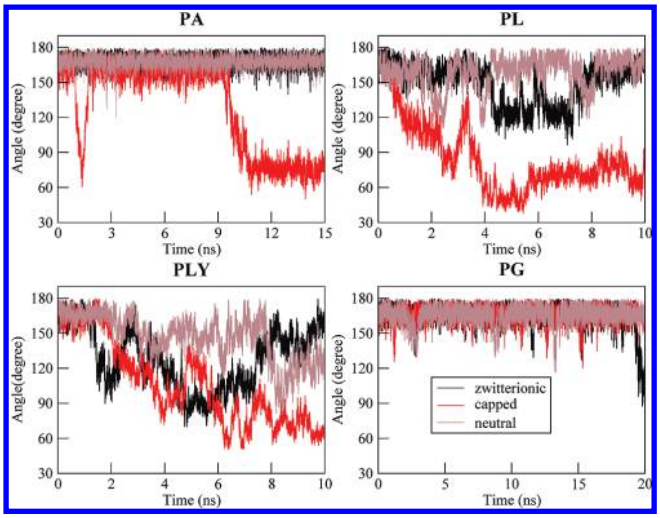

Figure 8. Angle between the two vectors as a function of time.

be observed in Figure 8. For capped PA and PL, the angle deviates from linearity much faster than any other forms of the same peptide. Since the capping has been done with $-NHCH_3$ at the C-terminal and with $-COCH_3$ at the N terminal, it makes the helical chain uniform. Therefore, the C═O and NH groups of the terminals can also get involved in the H-bonding within the α-helical backbone which is not possible for the zwitterionic and neutral forms. The change in angle between the vectors to less than 180° for the capped forms of the helices indicates that the side chains protruding out of the helical backbone come close to each other. Due to this, a stabilizing nonbonded interaction is developed among the side chains. Being uniform, the capped helix has the possibility to unwind from any point of the helix. However, the stabilization due to the nonbonded interactions among the side chains coming close to each other drives the unwinding pathway from the middle of the helical chain. In this regard, Sorin et al.,[11] in their study with capped homopolymeric helices, have observed that unfolding of the helices initiates by breakage of helices into multiple helical segments. This nonbonded interaction is dominated by interresidual H-bonding among the side-chain $-NH_2$ groups in all the forms of PLY helices (Figure 4). Due to higher fluctuations of helical backbone in some cases, mainly the capped form of PA and PL, and all the forms of PLY, the long-range nonbonded interactions get favorable and hence the helices start to unwind from the middle.

We have proposed in our previous report[16] that it is the higher fluctuations of the terminal residues that triggers the unwinding of the zwitterionic helices from the terminals. However, in Figure 3, the fluctuations can be observed to be higher for the terminal residues for all the helices studied in the first interval of time, e.g., 0−5 ns for capped PA or 0−1 ns for capped PLY. Thus, the factor of higher fluctuation of the terminal residues exists in all forms of the helices. In addition to this, the stabilizing long-range nonbonded interactions among the side chains exits due to higher fluctuations of backbone. Either of these two becomes a dominating factor during the unwinding process. All the PG helices unwind from the terminals. Hence, we can propose that the unwinding from middle for capped PA and PL helices is caused by more dominating stabilizing long-range nonbonded interactions among the side chains. That is, the capped PA and PL helices start to unwind from the terminals due to higher fluctuations of

dx.doi.org/10.1021/jp301556x | J. Phys. Chem. B 2012, 116, 4731−4740

the terminal residues but then the stabilizing long-range nonbonded interactions among the side chains predominate and the helices unwind from the middle.

CONCLUSION

Classical molecular dynamics simulations of the various forms of α-helical PA, PL, PLY, and PG in water at 300 K show sharp distinctions in their unwinding mechanisms. The distinctions in the unwinding mechanisms were extracted and analyzed to understand their source. The neutral forms of PA and PL helices unwind from the terminals akin to their zwitterionic analogue. However, their capped forms unwind from the middle of the α-helical chain due to higher fluctuation in the backbone and favorable nonbonded interactions among the side chains. All the forms of the PLY helices show interresidual H-bonding among the side-chain $-NH_2$ groups, which drives the unwinding of the PLY helices from the middle of the α-helical chain. Higher fluctuations of the terminal residues cause all the forms of PG helix to unwind from the terminals. No interresidual H-bonding exists among the side-chain $-COOH$ groups in any of the PG helices. Calculation of electrostatic interaction energy for the interaction between water and NH on peptide backbone shows that the interaction with water is more stabilizing. In addition to the higher fluctuations of the terminal residues, the H-bonding interactions with water molecules are also a determining factor for the unwinding of α-helical homopolymeric peptides.

Though higher fluctuations of the terminal residues and H-bonding interactions with water are the key factors determining the unwinding mechanism, but stabilizing long-range nonbonded interactions may favor for the unwinding from middle. For example, the capped PA and PL helices, and all forms of the PLY helices, start to unwind from the terminals due to higher fluctuations of the terminal residues but the unwinding is not relayed to the middle. Due to stabilizing long-range nonbonded interactions among the side chains, they eventually unwind from the middle. Similar results from multiple simulations signify that the mechanism of unwinding is statistically robust. Though the unwinding time scales in the multiple runs vary in the 2−4 ns range, the unwinding pathways are similar.

We have considered 30 amino acid long chains of the α-helix in all our simulations. Chain length is an important factor which may also dictate the unwinding mechanisms. Couch et al. have studied the helical contents of polyalanine peptides by varying the length of helix from 10 to 40 residues.[33] Increasing length of the chain also affects the flexibility of an α-helix.[34] Hence, further understanding is needed for longer chain length helical peptides. Choe et al. have shown that the bending modulus of helices is independent of the amino acid sequence.[35] The long-chain simulations with explicit solvent are difficult taking all atomistic details into account, as the system size will be very large. For such simulations, coarse graining can be an option. Further, all the PLY and PG simulations were performed taking side chains as $-NH_2$ and $-COOH$, respectively. For a more complete understanding, simulations of these systems need to be performed at different protonated states. Also, the unwinding mechanisms of helices constructed of combination of amino acids needs to be understood on the basis of our finding.

ASSOCIATED CONTENT

Supporting Information

Plot of potential energy of the whole system as a function of time. Also, evolution of the electrostatic interaction energy (depicted in Figure 7) with time is provided. Distance distribution plots similar to Figure 2 is provided for two more simulations. Plots for correlation between ratio of number of helix-forming H-bonds to nonhelical H-bonds and peak heights of HB-count plots at different intervals of time are given for two more simulations. This material is available free of charge via the Internet at http://pubs.acs.org.

AUTHOR INFORMATION

Corresponding Author

*E-mail: pr.pandey@ncl.res.in. Tel.: +91 (020) 25903148. Fax: +91 (020) 25902636

Notes

The authors declare no competing financial interest.

ACKNOWLEDGMENTS

We gratefully acknowledge CSIR and NCL for financial support of the project. S.R. gratefully acknowledges the Center for Excellence in Scientific Computing, NCL, for financial support and computational time.

REFERENCES

(1) Pauling, L.; Corey, R. B.; Branson, H. R. *Proc. Natl. Acad. Sci. U.S.A.* **1951**, *37*, 205−211.
(2) Chakrabartty, A.; Baldwin, R. L. *Adv. Protein Chem.* **1995**, *46*, 141−176.
(3) Maison, W.; Arce, E.; Renold, P.; Kennedy, R. J.; Kemp, D. S. *J. Am. Chem. Soc.* **2001**, *123*, 10245−10254.
(4) Kennedy, R. J.; Walker, S. M.; Kemp, D. S. *J. Am. Chem. Soc.* **2005**, *127*, 16961−16968.
(5) Job, G. E.; Kennedy, R. J.; Heitmann, B.; Miller, J. S.; Walker, S. M.; Kemp, D. S. *J. Am. Chem. Soc.* **2006**, *128*, 8227−8233.
(6) Zagrovic, B.; Jayachandran, G.; Millett, I. S.; Doniach, S.; Pande, V. S. *J. Mol. Biol.* **2005**, *353*, 232−241.
(7) Podtelezhnikov, A. A.; Wild, D. L. *Proteins: Struct., Funct., Bioinf.* **2005**, *61*, 94−104.
(8) Agostini, F. P.; Soares-Pinto, D. D. O.; Moret, M. A.; Osthoff, C.; Pascutti, P. G. *J. Comput. Chem.* **2006**, *27*, 1142−1155.
(9) Diana, D.; Ziaco, B.; Scarabelli, G.; Pedone, C.; Colombo, G.; D'Andrea, L.; Fattorusso, R. *Chem.—Eur. J.* **2010**, *16*, 5400−5407.
(10) Asciutto, E. K.; Mikhonin, A. V.; Asher, S. A.; Madura, J. D. *Biochemistry* **2008**, *47*, 2046−2050.
(11) Sorin, E. J.; Pande, V. S. *Biophys. J.* **2005**, *88*, 2472−2493.
(12) Garcia, A. E.; Sanbonmatsu, K. Y. *Proc. Natl. Acad. Sci. U.S.A.* **2002**, *99*, 2782−2787.
(13) Nymeyer, H.; Garcia, A. E. *Proc. Natl. Acad. Sci. U.S.A.* **2003**, *100*, 13934−13939.
(14) Garcia, E., A. *Polymer* **2004**, *45*, 669−676.
(15) Brooks, C.; Case, D. A. *Chem. Rev.* **1993**, *93*, 2487−2502.
(16) Pandey, P. R.; Roy, S. *Chem. Phys. Lett.* **2011**, *514*, 330−335.
(17) Nick Pace, C.; Martin Scholtz, J. *Biophys. J.* **1998**, *75*, 422−427.
(18) DiCapua, F. M.; Swaminathan, S.; Beveridge, D. L. *J. Am. Chem. Soc.* **1990**, *112*, 6768−6771.
(19) DiCapua, F. M.; Swaminathan, S.; Beveridge, D. L. *J. Am. Chem. Soc.* **1991**, *113*, 6145−6155.
(20) Baldwin, R. L. *Proteins: Struct., Funct., Bioinf.* **2011**, *79*, 2021−2026.
(21) Baldwin, R. L. *J. Biol. Chem.* **2003**, *278*, 17581−17588.
(22) Van Der Spoel, D.; Lindahl, E.; Hess, B.; Groenhof, G.; Mark, A. E.; Berendsen, H. J. C. *J. Comput. Chem.* **2005**, *26*, 1701−1718.
(23) Hess, B.; Kutzner, C.; van der Spoel, D.; Lindahl, E. *J. Chem. Theory Comput.* **2008**, *4*, 435−447.

(24) Kaminski, G. A.; Friesner, R. A.; Tirado-Rives, J.; Jorgensen, W. L. *J. Phys. Chem. B* **2001**, *105*, 6474−6487.
(25) Duan, Y.; Wu, C.; Chowdhury, S.; Lee, M. C.; Xiong, G.; Zhang, W.; Yang, R.; Cieplak, P.; Luo, R.; Lee, T.; Caldwell, J.; Wang, J.; Kollman, P. *J. Comput. Chem.* **2003**, *24*, 1999−2012.
(26) Jorgensen, W. L.; Chandrasekhar, J.; Madura, J. D.; Impey, R. W.; Klein, M. L. *J. Chem. Phys.* **1983**, *79*, 926−935.
(27) Berendsen, H. J. C.; Postma, J. P. M; van Gunsteren, W. F.; Dinola, A.; Haak, J. R. *J. Chem. Phys.* **1984**, *81* (8), 3684−3690.
(28) Patra, M.; Karttunen, M.; Hyvonen, M. T.; Falck, E.; Lindqvist, P.; Vattulainen, I. *Biophys. J.* **2003**, *84* (6), 3636−3645.
(29) Li, W.; Qin, M.; Tie, Z.; Wang, W. *Phys. Rev. E* **2011**, *84*, 041933-1−041933-9.
(30) Doruker, P.; Bahar, I. *Biophys. J.* **1997**, *72*, 2445−2456.
(31) Avbelj, F.; Luo, P.; Baldwin, R. L. *Proc. Natl. Acad. Sci. U.S.A.* **2000**, *97*, 10786−10791.
(32) Baldwin, L., R. *Biophys. Chem.* **2002**, *101*−*102*, 203−210.
(33) Couch, V. A.; Cheng, N.; Nambiar, K.; Fink, W. *J. Phys. Chem. B* **2006**, *110*, 3410−3419.
(34) Lakkaraju, S. K.; Hwang, W. *Phys. Rev. Lett.* **2009**, *102*, 118102-1−118102-4.
(35) Choe, S.; Sun, S. X. *J. Chem. Phys.* **2005**, *122*, 244912-1−244912-9.